Hindawi
International Journal of Photoenergy
Volume 2018, Article ID 7630390, 12 pages
https://doi.org/10.1155/2018/7630390

Research Article

Optimization Design of a Multibusbar Structure: The Using of a Conductive Belt

Han Han,[1] **Yelong Wu**,[1,2] **and Chao Ma**[1]

[1]*Shaanxi Key Laboratory of Quantum Information and Quantum Optoelectronic Devices, Xi'an Jiaotong University, Xi'an, Shaanxi 710049, China*
[2]*Key Laboratory of Nonequilibrium Synthesis and Modulation of Condensed Matter, Ministry of Education, Xi'an Jiaotong University, Xi'an, Shaanxi 710049, China*

Correspondence should be addressed to Yelong Wu; yelongwu@xjtu.edu.cn

Received 4 February 2018; Revised 2 June 2018; Accepted 27 June 2018; Published 25 July 2018

Academic Editor: Mohammed Ashraf Gondal

An interconnect electrode called conductive belt was applied to modules instead of interconnection ribbons. The conductive belt has multiple wires and can achieve a multibusbar structure by forming ohmic contacts with the cell electrodes. The following problems were studied with innovative approaches to optimize the multibusbar modules: the shading rate and the contact resistance of the conductive belts, the relationship between the finger series resistance and the wire number, and the influence of the series resistance variation on the maximum power output. Furthermore, the wire number and diameter were optimized according to the following conditions: the cell sizes were full, half, and one-third, and the finger wet weights of a full cell were 80 mg, 40 mg, and 20 mg. The result showed that multibusbar and half-cell structures could achieve the maximum power output, the wire number was 16 and the wire diameter was 200 μm, and the finger wet weight was reduced to 20 mg. Finally, the reliability of the modules made with conductive belts was tested and was qualified according to International Electrotechnical Commission standards.

1. Introduction

Adding more busbars can shorten the effective finger length and reduce the series resistance (R_s) of the module [1]. Compared to the conventional three-busbar modules, it has been calculated that if the total width of busbars remains unchanged, multibusbar (MBB) design can increase the absolute efficiency by 0.33% [2] or 0.5% [3]. Because MBB is less dependent on finger resistance [4], the finger wet weight can be reduced [5], or the silver can be replaced with other materials such as nickel, which is much less expensive and may have better contact with the cell [6].

To date, the busbar number of the conventional modules has grown from three to four or five, and the width of the interconnection ribbons has decreased to 0.9 mm. Making interconnection ribbons even narrower is difficult, and if more busbars are added, the module efficiency would drop because of the increase in shading loss. Using copper wires instead of interconnection ribbons can reduce the busbar width to less than 0.3 mm; thus, the busbar number can be increased. On the other hand, copper wire can reflect a part of the incident light back to the cell, which will decrease its shading loss [7].

Soldering copper wires onto the silver pads of the cells with Sn alloy can achieve an MBB structure. Increasing the pad area [8] or plating silver onto the pads [9] can increase the peel force of the wires, and the robustness of the wires has proven its reliability [10]. However, the front pads of the cells shade the incident light, and the heated soldering process may increase the breakage rate of the cells. Another MBB technique called SmartWire Connection Technology (SWCT) can avoid the problems noted above: the cell busbars are removed, and the wires are pressed onto the cells by composite films during encapsulation and form ohmic contacts with the fingers. The wires have low-melting-point coatings, which can increase contact reliability [11]. Several optimizations of this technique have been carried out: the fingers could be designed to be dotted lines, and the diameter

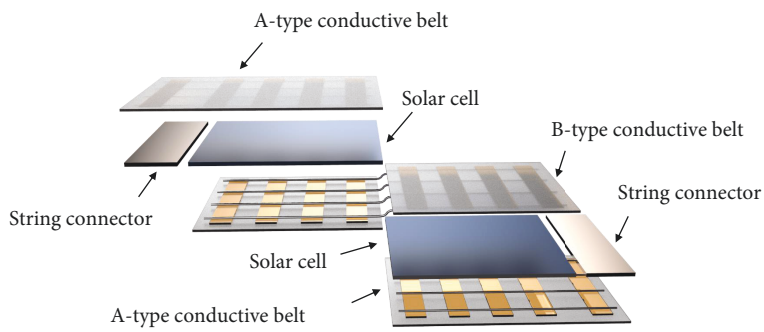

Figure 1: The structure and the connect mode of the conductive belts.

of the interconnect wires was 0.3 mm [12]; the composite film that covers the wires was thermoplastic polyolefin (TPO), whose reliability was determined [13]; the back electron pattern of the cell was optimized, and the wires could connect to the back electrode of the cell in different directions [14]; the finger wet weight could be sharply reduced by applying inkjet printing [15] or plating [16] instead of screen printing; and plating Sn on the surface of fingers could achieve a better contact [11]. However, if this busbarless design is used for commercial purposes, there are some issues that need to be resolved: (1) The soldering reliability. For the busbarless solar cell, the copper wires can only be soldered with the fingers, and the soldered area is reduced by 90% compared with conventional solar cells with busbars, which will lead to a significant reduction of soldering reliability. (2) The copper wires and the cells are soldered during the lamination process. The oxide layer of the finger surface should be removed, and the organic residue generated during the soldered process needs to be deduced, which will increase the cost. (3) The design of the composite film which covers the wires. The sun-light transmittance of the composite film in the solar modules need to be more than 99%. It is necessary to increase the light transmittance and reduce the thickness, and the refractive index needs to match the material of the upper and lower layers. However, reducing the thickness of the film will reduce its hardness, which will increase the difficulty of module manufacture.

The laminated grid cell (LGCell) is mainly suitable for heterojunction solar cells with transparent conducting oxide (TCO) layers on the surface [17, 18]. The transparent conductive polymer (TCP) and the copper wires are attached to the TCO layer successively. Because the silver electrode is completely removed, the manufacturing cost can be significantly reduced. However, the sun-light transmittance of the TCP layer and the contact resistance of the TCP and the TCO need to be optimized.

Half-cell design can decrease 50% of module current and reduce the resistance power loss of interconnection ribbons by 75%. The added cell gaps can reflect a part of the incident light back to cells and increase the output power of modules [19]. The cell cutting process will lead to a bit loss in mechanical strength and electrical properties [20], and the loss can be reduced to negligible levels by the thermal laser separation process [21, 22]. In total, half-cell design can demonstrate an increase in power output of about 5% [23].

In this study, an interconnecting electrode called conductive belt was applied instead of interconnection ribbons. The conductive belt had a certain number of wires and could achieve an MBB structure. To optimize the number and the diameter of the wires, several experiments were designed to test the following parameters: the resistance and the shading loss of different parts of the module electrode and the influence of the series resistance variation on the power output. The module electrode was optimized according to the current technological levels in photovoltaic industry development, and a 16-wire structure with a diameter of 200 μm combined with half cell was proved to achieve the most power output.

2. Materials and Feasibility Test

2.1. Introduction to Conductive Belts. The conductive belt has three layers: wires, composite films, and support films. The composite films have several separate parts and are used to press the wires onto cells or string connectors. The support films are used to load the wires and the composite films. Figure 1 shows two types of conductive belts. The A type is used to connect cells to string connectors, where the two contact surfaces are on the same side, and the support film is successive. The B type, which connects the adjacent solar cells, has two parts, and both parts have three layers. In the left part, from top to bottom are wires, composite films, and support films. The wires extend to the right part. The composite films and the support films are ordered upon the right part of the wires. As shown in Figure 1, the cells, conductive belts, and string connectors are laid successively, and after laminating the wires form ohmic contacts with the cells or the string connectors.

The cross section of a conductive belt combined with a cell is shown in Figure 2. Compared to SmartWire Connection Technology, the structure of the conductive belt is more complex, but it can reduce the cost and increase the transmittance. The support film is made of the same material with the same thickness as the module-encapsulated adhesive film, that is, ethylene-vinyl acetate copolymer (EVA) with 0.3 mm thickness. Through laminating, the support

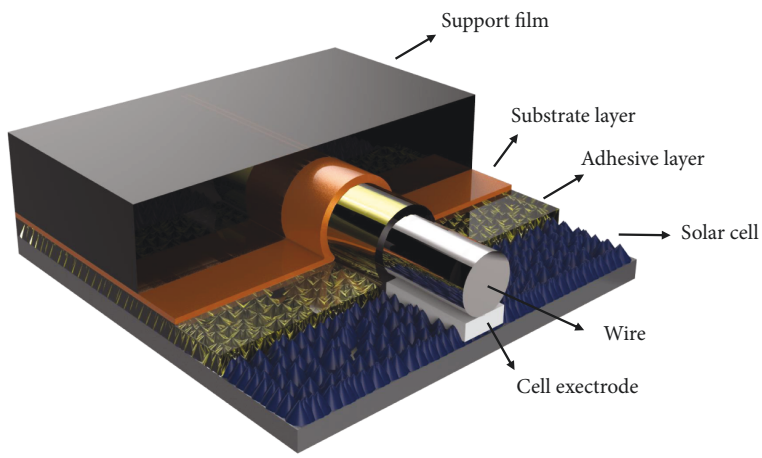

Figure 2: Cross section of the combined structure of a conductive belt and a cell.

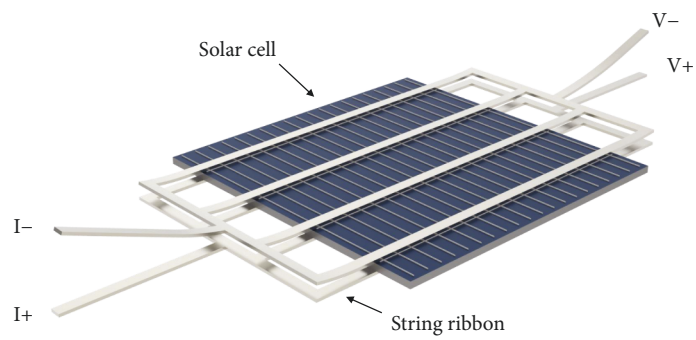

Figure 3: Schematic of the connect mode of the I–V tester to the cells soldered with interconnection ribbons.

film is integrated into the encapsulated adhesive film. The total EVA usage in the modules does not need to be increased. Thus, the support film will neither increase the cost of the module nor increase the shading of the incident light. The composite film is composed of a substrate layer and an adhesive layer. The substrate layer is used to separate the support film and the wires, and it must have a high sunlight transmittance and a strong anti-ultraviolet aging ability. Ethylene tetrafluoroethylene (ETFET) is the most suitable material, but the cost is too high. Therefore, the thickness of ETFET is reduced to less than 40 μm, making its cost more acceptable. The adhesive layer is used to fill the gap between the substrate layer and the cell surface. Its main component is EVA, and the thickness is 20 μm. In order to further reduce the cost and shading losses, the composite film is designed as a hollow structure and only covers the copper wire.

As the busbar is removed, SiN cannot be soldered well; that is, traditional soldering reliability will be greatly reduced. Therefore, the conductive adhesive not only is used to coat the copper wire instead of tin-bismuth alloy but also can effectively bond with the fingers and SiN. The curing temperature is lower than 150°C, and the curing time is less than 30 s. During the lamination process, it forms a reliable contact with the cells.

2.2. Transmittance Test. The composite film and the support film of the conductive belt remain unchanged, but the wire number and wire diameter will be adjusted to match the cell size and the conductivity of the fingers. And a part of the incident light on the wires can be reflected back into the cell [24]. An experiment was carried out to test the transmittance of the conductive belt with different numbers of wires: 25 pieces of p-type, silicon monocrystalline solar cells with four busbars were chosen. The size of the solar cells is 156*156 mm^2. For each cell, the interconnection ribbons were soldered onto the front and back busbars and extended out of the cells, as shown in Figure 3. The extended interconnection ribbons of the two surfaces were isolated by electric tape. The current–voltage (I–V) curves of the soldered cells were tested by an I–V tester. The front current and voltage test leads for the I–V tester were I^- and V^-, and the back current and voltage test leads for the I–V tester were I^+ and V^+. As shown in Figure 3, the test leads of the I–V tester were connected to different ends of the interconnection ribbons. The R_s tested by this connect mode only include the cell series resistance and the contact resistance (R_c) of the interconnection ribbons to the cell. This test mode could reduce the test error from the resistance of the interconnection ribbons and the contact resistance of the interconnection ribbons to the test leads.

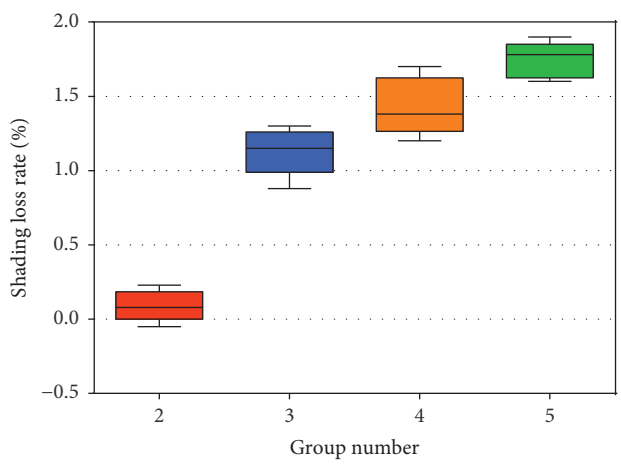

Figure 4: The shading rate of the conductive belts for groups 2 to 5.

The soldered cells were divided into five groups numbered 1 to 5, and each group had five cells. The cells of group 1 were encapsulated into conventional one-cell modules directly. The other cells were encapsulated into one-cell modules with A-type conductive belts on the front of the cells. Shading loss mainly affected photogenerated current. To test the shading loss of the conductive belt precisely and minimize its influence on the module resistance, the wires of the conductive belts did not contact with the cell electrode. The wire numbers and the wire diameters were changed by groups: group 2 had no wires; groups 3, 4, and 5 had 15 wires, and the wire diameters of each group were 150 μm, 200 μm, and 250 μm, respectively. The I–V curves of the modules were tested with the connect mode unchanged. The light source was 1000 W/m^2 and AM 1.5, and the test temperature was 25°C. For group x, $x = 1$ to 5. The average short current (I_{sc}) of the soldered cells before and after encapsulating was named I_x and I'_x. The shading rate of the conductive belt (S_x) could be expressed as

$$S_x = \frac{I'_1}{I_1} - \frac{I'_x}{I_x}. \quad (1)$$

The average shading rates tested for each group are shown in Figure 4. The total shading rate of the composite film and the support film was S_{film}. As could be calculated from Figure 4, $S_{\text{film}} = 0.08\%$. The shading rate of the conductive belt with 150 μm wire is 1.08%, so the shading rate of the wires is about 1%. The wire coverage rate is the wire diameter multiplied by the wire number and divided by the cell width. As could be calculated, the shading rate is 70% of the coverage rate. The same conclusion can also be obtained for 200 μm and 250 μm wires. Thus, the shading rate of the wires (S_{wire}) could be expressed as

$$S_{\text{wire}} = \frac{0.7nD}{W}. \quad (2)$$

W is the width (perpendicular to the cell-connecting direction) of the cell. D and n are the diameter and the number of the wires, respectively. The power loss of the conductive belts caused by shading the incident light (P_{cs}) could be expressed as

$$P_{cs} = (S_{\text{film}} + S_{\text{wire}})P_{\text{m}}. \quad (3)$$

P_{m} is the module maximum power output. As can be seen from the experiment results, the main shading rate of the conductive belt is from the wires, and since the wire coating has a high reflectivity, 30% of the wire incident light can be reflected back into the cells.

2.3. Contact Resistance Test. The wire contact resistances to fingers were measured by the following experiments. Ten one-cell modules were made with conductive belts. The front structure of the modules is shown in Figure 5(a). There were two wires at the right and left quarter positions of the cell. The wire diameter was 250 μm, and the distance between the adjacent two wires was about 2 mm. The back electrode and back connect mode were the same as those in Figure 3. Each module was tested as follows. We kept the lower terminals of the two left wires connected to the I$^-$. First, we connected the upper terminal of the two left wires to the V$^-$ and tested the I–V curve, and the module series resistance tested was R_{s1}. The test method was comparing two I–V curves measured at 500 W and 1000 W illumination intensities [25]. Then, we connected the upper terminal of the two right wires to the V$^-$ and tested the I–V curve, and the module series resistance tested was R_{s2}. In the one-cell module, all the 4 wires were 160 mm long. The 3 ribbons which connect to the wires had the same length of 165 mm. Therefore, the wire resistance could hardly have contribution to $R_{s1} - R_{s2}$. The first test mode tested the voltage of the wires, and the second test mode tested the voltage of the fingers. Thus, $(R_{s1} - R_{s2}) \times 2$ is equal to the sum of the contact resistance of one wire to the fingers and the resistance of the fingers between the adjacent two wires.

The wire contact resistances to the back busbars and to the Al-BSF were also tested by the same method, and 10 one-cell modules were made, respectively. The front electrode and the front test mode of the modules were the same as those in Figure 3. The back electrode and the back test modes are shown in Figures 5(b) and 5(c). In Figure 5(b), $(R_{s1} - R_{s2}) \times 4$ is equal to the sum of the contact resistance of one wire to the back busbars and the resistances of the back busbars between the adjacent two wires. In Figure 5(c), $(R_{s1} - R_{s2}) \times 2$ is equal to the sum of the contact resistance of one wire to the Al-BSF and the resistances of the Al-BSF between the adjacent two wires.

The $R_{s1} - R_{s2}$ tested from the three experiments are shown in Figure 6. All the $R_{s1} - R_{s2}$ tested are less than 0.45 mΩ. Thus, the contact resistance of one wire to the fingers and Al-BSF was less than 0.9 mΩ and the contact resistance of one wire to the back busbars was less than 1.8 mΩ. Contact resistance is inversely proportional to the wire number. If the wire number increases to more than eight, the wire contact resistances to fingers and Al-BSF can be reduced to less than 0.1 mΩ, and the resulting power loss can be ignored. In addition, the wires can contact with fingers and Al-BSF instead of front and back busbars. Thus, front and back

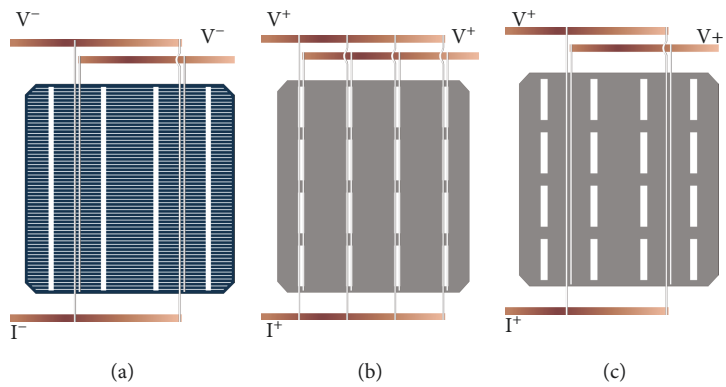

Figure 5: Schematic of the test modes to analyze the wire contact resistance to different parts of the cell electrode. (a) Fingers, (b) back busbars, and (c) Al-BSF.

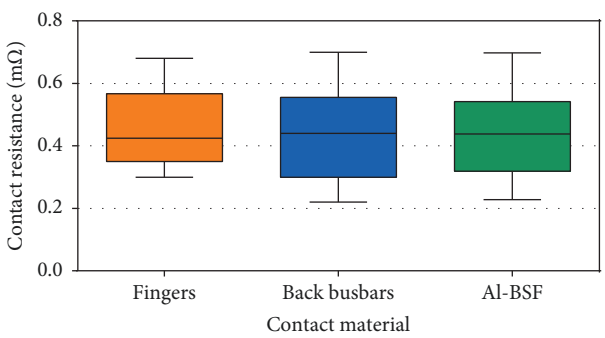

Figure 6: The $R_{s1} - R_{s2}$ tested from the fingers, back busbars, and Al-BSF.

busbars can be removed, which will improve open circuit voltage (V_{oc}) and reduce the cost of the silver electrode.

3. Analysis of Finger Series Resistance

3.1. Finger Series Resistance Measured by a 6½-Digit Multimeter. The series resistance of the fingers (R_f) can be expressed as [26]

$$R_f = \frac{R_0}{12mn^2}. \tag{4}$$

R_0 is the resistance of a whole finger, m is the finger number, and n is the busbar number. Thirty conventional four-busbar crystalline solar cells produced by screen printing currently were chosen as samples. The average width and thickness of their fingers were tested and were 55 μm and 15 μm, respectively. The finger number was 105. The finger resistance was measured by the following experiment: the cells were separated by laser scribing and subsequent cleaving. The separated part of the cell had one full finger, and the four busbar areas of the finger were numbered 1, 2, 3, and 4. A 6½-digit multimeter was used to contact with the busbar areas and to test the finger resistance. Suppose $x = 1$, 2, 3, 4, the tested resistance between the busbar areas of number x and number $x + 1$ was $R_{x(x+1)}$, the contact resistance of the 6½-digit multimeter probe to the busbar area of number x was R_{cx}, the finger line resistivity between the busbar areas of number x and number $x + 1$ was $\rho_{x(x+1)}$. R_{cx} and $\rho_{(x-1)x}$ could be represented by the following equations:

$$R_{cx} = \frac{R_{(x-1)x} + R_{x(x+1)} - R_{(x-1)(x+1)}}{2}, \tag{5}$$

$$\rho_{(x-1)x} = \frac{R_{(x-1)x} - R_{c(x-1)} - R_{cx}}{l} \tag{6}$$

In (5), $x = 2, 3$. In (6), $x = 3$, and l is the distance between the adjacent two busbar areas. For conventional 156 mm cells, $l \approx 38$ mm. The resistivity of the diffusion layer under the fingers was about 1000 times higher than that of the fingers, and the impact of its shunting could be ignored. For each cell, finger line resistivity of different positions was tested by the above method, and the average linear resistivity was about 58 mΩ/mm, and the resistance of a whole finger was 9 Ω. According to (4), the series resistance of 105 fingers with four busbars was 0.45 mΩ.

3.2. Finger Series Resistance Measured by I–V Tester. Two four-busbar monocrystalline solar cells with similar I–V curves were chosen to make two one-cell modules by applying conductive belts. Before encapsulation, I–V curves of the two cells were tested by the I–V tester with four rows of probes, and the cell series resistances tested were R_{s1} and R_{s2}. The front electrode structures of the modules are shown in Figure 7(a). The left structure had two wires on the middle position of the cell, and the distance between the two wires was 2 mm. The right structure had two wires, and the wires were located on the two quarter positions of the cell, respectively. Two string connecters contacted with the two ends of the wires, respectively, and extended from the modules. The V^- and I^- test leads of the I–V tester connected to the upper and the lower string connecters of the front electrode as shown in Figure 7(a). The irrelevant resistance includes the contact resistance of the wires to the string connecters, and the contact resistances of the test leads to the string connecters; the wire resistance and the string connecter resistance could thus be avoided in the test result. The back structure and the back test mode of the two modules were the same as those in Figure 3, and the series resistances of

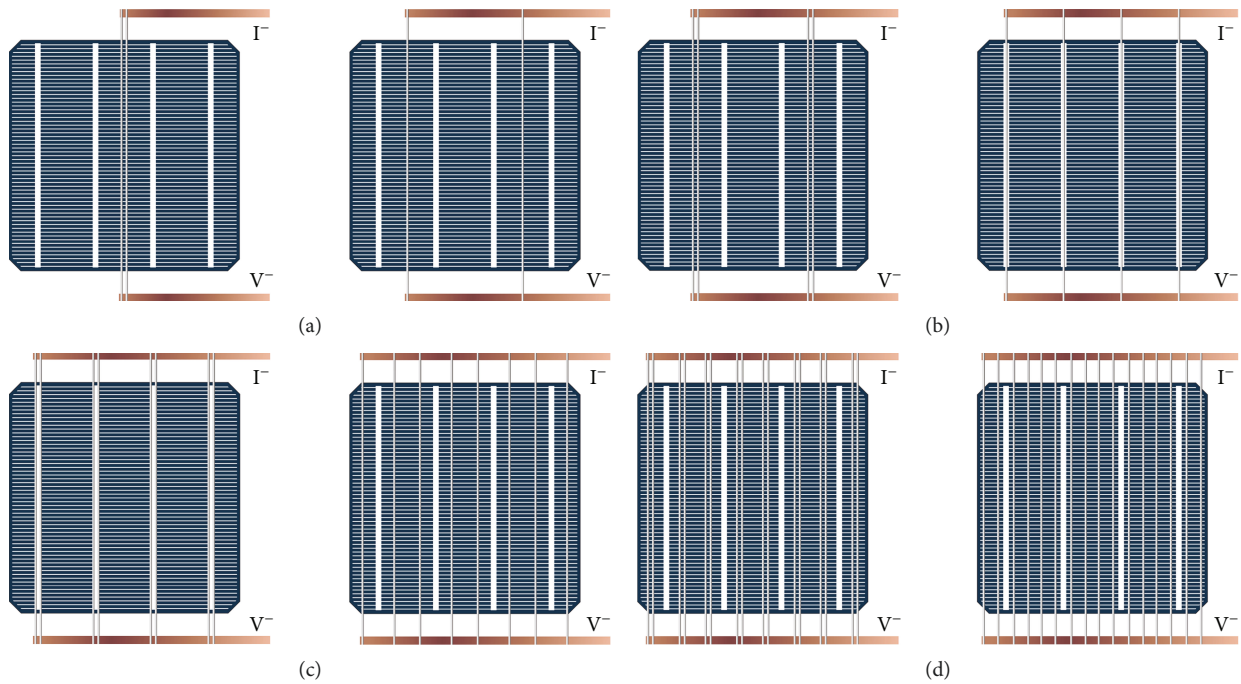

Figure 7: Four groups of module electrode structures were designed to test the finger series resistance; each group had two module electrode structures with different busbar numbers. (a) one and two busbars, (b) two and four busbars, (c) four and eight busbars, and (d) eight and sixteen busbars.

the two modules tested were R_{s3} and R_{s4}. The difference of the series resistance (ΔR_s) caused by the different wire positions of the two modules could be expressed as

$$\Delta R_s = R_{s3} - R_{s4} - R_{s1} + R_{s2}. \quad (7)$$

In Figure 7(a), the left module structure had two wires on the middle position. The distance between the two wires was so small that the left module was equivalent to have one busbar. Similarly, the right module structure had two busbars. The two modules both had two wires, and the shading loss and the resistance of the conductive belt were the same. Thus, the difference of the series resistance was from the finger series resistance caused by different busbar numbers. Suppose that the series resistance of the fingers with four busbars was R_{s0}; according to (4), the ΔR_s of the left and right module structures should be equal to $12R_{s0}$. Another three groups of modules were made and tested in the same way, and the structures of each group are shown in Figures 7(b)–7(d). The ΔR_s of each group was also calculated with (4). In Figure 7(b), ΔR_s should be equal to 3 R_{s0} due to the difference of two and four busbars. In Figure 7(c), ΔR_s should be equal to $3R_{s0}/4$ due to the difference of four and eight busbars. In Figure 7(d), ΔR_s should be equal to $3R_{s0}/16$ due to the difference of eight and sixteen busbars.

The above four experiments were repeated four times, and 32 one-cell modules were made and tested. For the four groups of module structures, the ΔR_s resulting from the four repeated experiments are shown in Figure 8. The ΔR_s calculated with (4) are also shown in Figure 8. The ΔR_s that got through the two ways were approximately identical. The result proves that (4) is accurate for calculating the series resistance of the fingers.

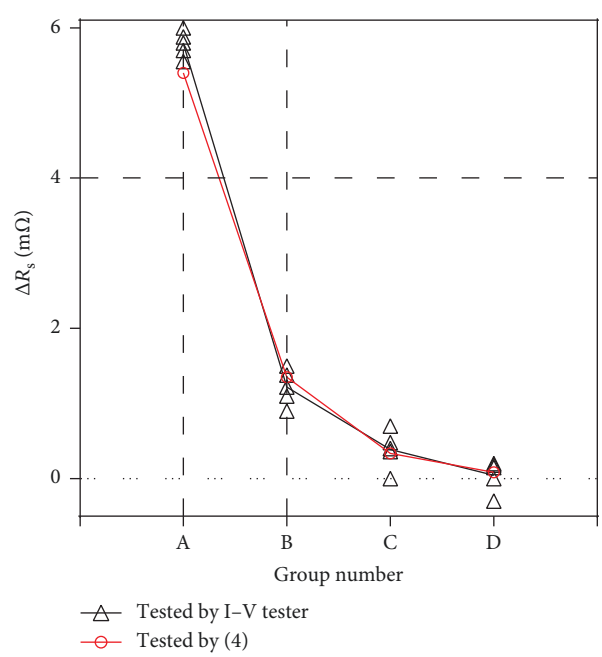

Figure 8: ΔR_s of different busbar numbers tested in two ways: (1) the series resistance of the four groups of modules with different busbar numbers was tested with the I–V tester, and the experiment was repeated four times, and (2) the series resistance of the fingers with different busbar numbers was calculated with (4).

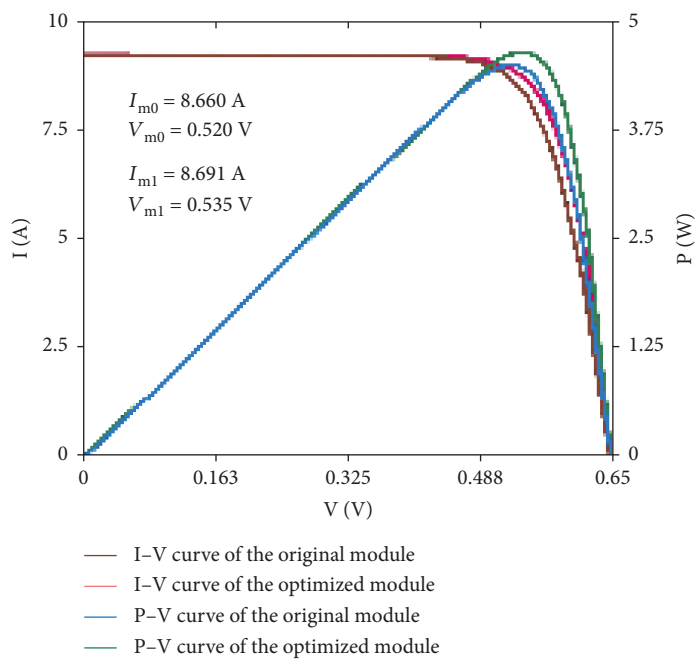

Figure 9: The I–V and P–V curves of the original and optimized modules.

3.3. Relationship between Series Resistance and Power Output. Series resistance power loss (P_s) can be expressed as [27]

$$P_s = R_s I_m^2. \tag{8}$$

I_m is the current at maximum power point. The relationship between the current (I) and the voltage (V) of the module is [28]

$$I(V) = I_{sc}\left[1 - \frac{\exp\left[q(V + I(V)R_s/nk_BT)\right] - 1}{\exp\left(qV_{oc}/nk_BT\right) - 1}\right] - \frac{V + I(V)R_s}{R_{sh}} \tag{9}$$

I_{sc}, R_{sh}, and T are the short circuit current, shunt resistance, and temperature of the module, respectively, k_B is the Boltzmann constant, and n is the ideality factor.

A standard one-cell module was chosen, and its electrical parameters were tested. The I_{sc} and V_{oc} of the module were 9.221 A and 0.641 V, respectively. V_m is the voltage at maximum power point; the I_m, V_m, and P_m of the module (I_{m0}, V_{m0}, and P_{m0}) were 8.660 A, 0.520 V, and 4.503 W, respectively, and $T = 300$ K. The I–V curve and the power–voltage (P–V) curve of the module were simulated, and the results are shown in Figure 9. As could be calculated with (9), the series resistance of the original module (R_{s0}) was 4.4 mΩ and $n = 1.119$. Suppose that the module electrode was optimized, and the optimization mainly decreased the module series resistance. The increment of the series resistance (ΔR_s) was −2 mΩ. The I–V and P–V curves of the optimized module were calculated again, and the results are also shown in Figure 9. The I_m, V_m, and P_m of the optimized module (I_{m1}, V_{m1}, and P_{m1}) were 8.691 A, 0.535 V, and 4.650 W.

For the original and optimized modules, the increment of P_s (ΔP_s) was calculated with (8) and can be defined as

$$\Delta P_s = (R_{s0} + \Delta R_s)(I_{m0} + \Delta I_m)^2 - R_{s0} I_{m0}^2. \tag{10}$$

$\Delta I_m = I_{m1} - I_{m0}$, and $\Delta I_m = 31$ mA. As could be calculated,

$$\frac{\Delta I_m}{I_{m0}} \ll \frac{\Delta R_s}{R_{s0}} \tag{11}$$

And (10) could be simplified to

$$\Delta P_s = \Delta R_s I_{m0}^2. \tag{12}$$

ΔP_s calculated with (10) and (12) were −0.149 W and −0.150 W, respectively. $\Delta P_m = P_{m1} - P_{m0}$, and $\Delta P_m = 0.151$ W. So $\Delta P_m \approx -\Delta P_s$.

Based on the above analysis, the influence of the series resistance variation on P_m was found: if $|\Delta R_s| < 2$ mΩ, ΔP_s can be calculated with (12), and ΔP_m was approximate to $-\Delta P_s$.

The following experiment was done to prove the above conclusion. A one-cell module was made. The front structure is shown in Figure 10, where the front interconnection ribbon extended from the lower side of the cell. Five points of the interconnection ribbon named A, B, C, D, and E were chosen, and all the resistances between the adjacent points (A and B, B and C, C and D, and D and E) of the sting ribbon were 0.5 mΩ. The back connect mode was the same as that in Figure 3. The I^- and V^- test leads of the I–V tester contact to the same point and test the I–V curve. This test was carried out five times, and the contact points were A, B, C, D, and E. The electrical parameters of each point were compared, and the comparison mode includes A versus B, B versus C,

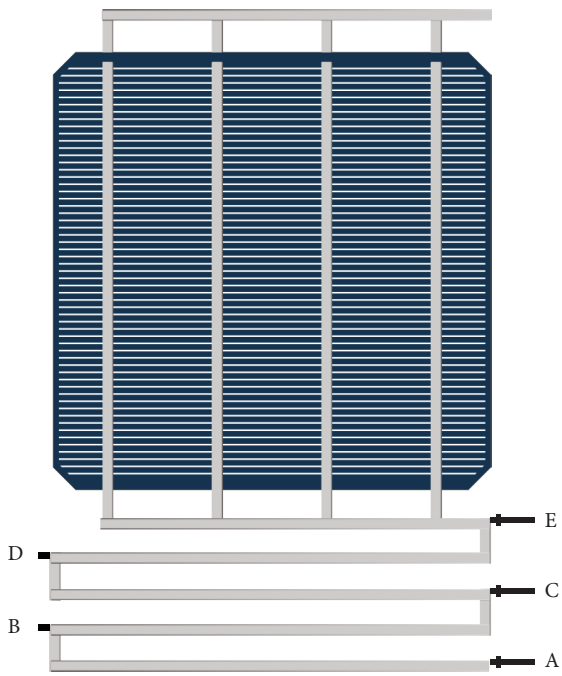

Figure 10: Sketch of the module electrode structure and test mode used to analyze the influence of the series resistance variation on P_m.

Table 1: ΔR_s, ΔI_m, ΔP_m, and ΔP_s between adjacent two points: ΔR_s, ΔI_m, and ΔP_m were tested by I–V tester; ΔP_s was calculated with (12).

Comparison mode	ΔR_s (mΩ)	ΔI_m (mA)	ΔP_m (mW)	ΔP_s (mW)
A versus B	0.49	−2.29	−38.25	36.81
B versus C	0.52	−2.46	−38.83	39.04
C versus D	0.51	−1.60	−36.26	38.27
D versus E	0.49	−1.77	−35.54	36.75

C versus D, and D versus E. The difference of R_s, I_m, and P_m (ΔR_s, ΔI_m, and ΔP_m) for each comparison mode is shown in Table 1. The ΔR_s for each comparison mode was approximate to the resistance between the adjacent points, which was 0.5 mΩ. So the rangeability of series resistance tested by the I–V tester was accurate. For each comparison mode, $|\Delta I_m| < 2.5$ mA, thus $\Delta I_m/I_m \ll \Delta R_s/R_s$, which was consistent with (11). So ΔP_s could be calculated with (12). The ΔP_s of each comparison mode can be seen in Table 1. For each comparison mode, the absolute difference between ΔP_m and $-\Delta P_s$ was less than 6%. Thus, ΔP_m was approximate to $-\Delta P_s$, and the above conclusion was proved.

4. Optimization of the Multibusbar Module Electrode

4.1. Relationship between the Optimized Wire Diameter and the Wire Number. The primary optimization of the MBB module electrode is in reducing the total power loss caused by the shading and the series resistance of the wires and fingers. MBB mainly reduces finger series resistance, and this decrement is less than 2 mΩ per cell; hence, ΔP_m caused by the decrement in series resistance is equal to $-\Delta P_s$, which can be calculated with (12). Suppose the wire electrical resistivity was ρ, the power loss caused by the shading and the resistance of the conductive belt is P_c, according to (3) and (8); the P_c of a module whose cell area is equal to a full cell can be obtained by

$$P_c = \left(\frac{4\rho L}{3n\pi D^2} + \frac{1}{(3n\pi D^2/4\rho L) + (3/R_\square)}\right) I_m^2 + \left(\frac{0.7nD}{W} + S_{\text{film}}\right) P_m. \quad (13)$$

L is the length of a full cell, which at present is about 156 mm. $R_\square$ is sheet resistance of Al-BSF. Al-BSF can share back current with the back wires. The Al-BSF sheet resistance of conventional cells was tested and was 20 mΩ. For different wire numbers, the wire diameters to achieve the lowest power losses were calculated, and the cell sizes were full, half, and one-third. The results are shown in Figure 11. The wire diameter could be reduced by decreasing the cell size or by adding more wires.

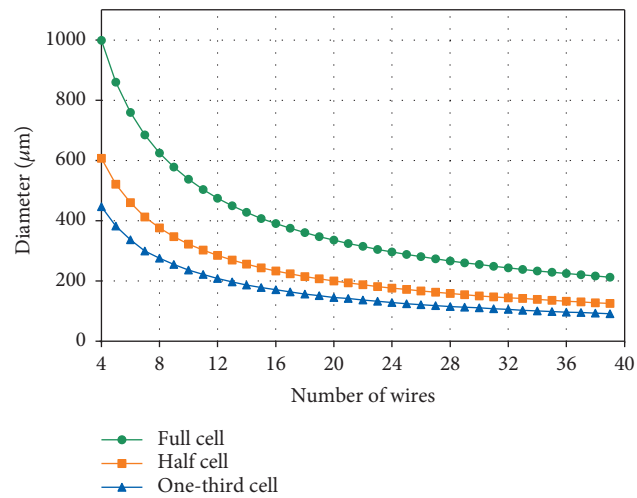

Figure 11: Relationship between the optimized wire diameters and the wire numbers for hull-, half-, and one-third-cell designs.

4.2. Power Loss Analysis of Multibusbar Combined with Different Cell Sizes. The power loss caused by the finger resistance (P_f) can be defined as

$$P_f = R_f I_m^2. \quad (14)$$

R_f can be obtained by (4), and in (4), R_0/m is inversely proportional to the wet weight of the fingers. Braun et al. [24] discussed the relationship between the Ag paste and busbar number: the optimized cell efficiency was 19.7%. The 3-busbar design needs a 108 mg Ag paste, while the 15-busbar solar cell design only needs 6.8 mg. Currently,

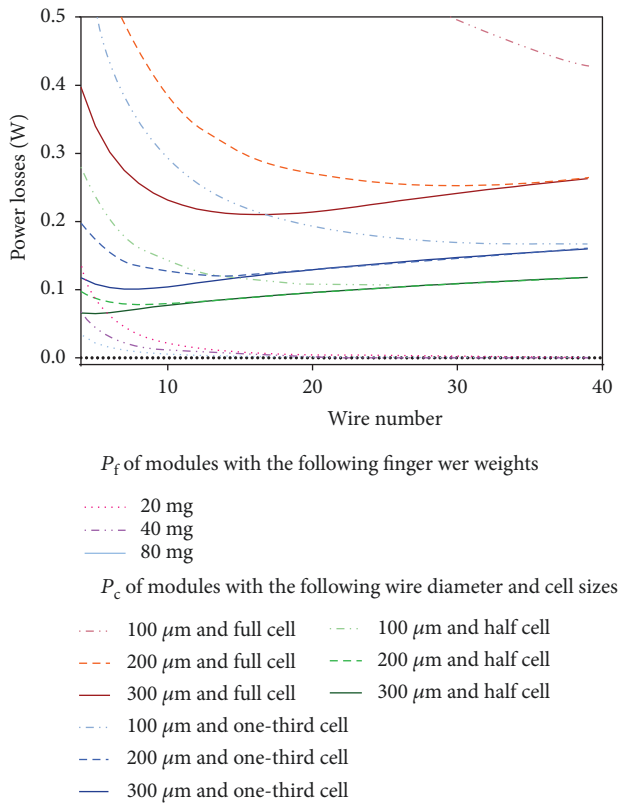

Figure 12: Relationship between the number of the wires and the following power losses of a module whose cell area is equal to a full cell: resistance power losses of fingers with wet weights of 80 mg, 40 mg, and 20 mg per full cell; power losses of conductive belts with wire diameters of 100 μm, 200 μm, and 300 μm, and with cell sizes of full, half, and one-third.

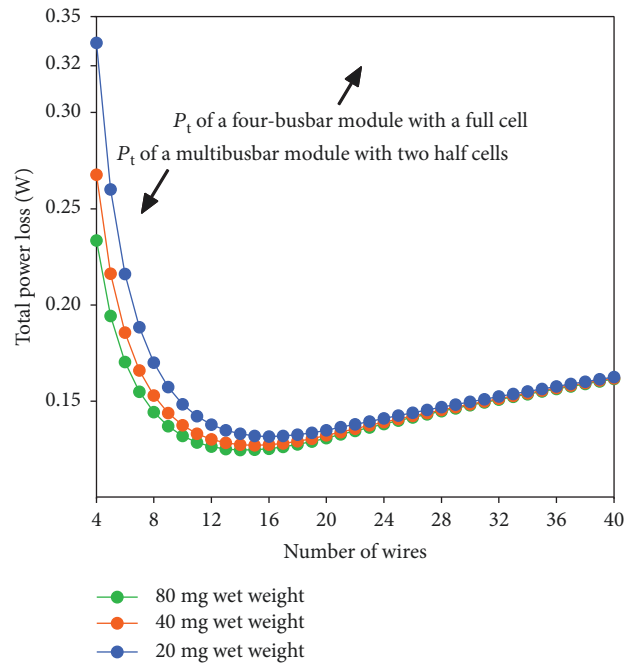

Figure 13: The P_t of three MBBHC modules and a conventional module: (1) multibusbar modules with two half cells, respectively, the wire numbers range from 4 to 40, and the finger wet weights are 80 mg, 40 mg, and 20 mg; (2) a four-busbar module with a full cell, whose finger wet weight is 80 mg.

the cell efficiency has increased to more than 21%, and P_f needs to be further reduced. The average wet weight of the fingers is about 80 mg per cell and can be reduced by decreasing the thickness or the width of the fingers. For the finger wet weights of 80 mg, 40 mg, and 20 mg, the relationship between P_f and the wire number was calculated with (14). The results are shown in Figure 12. To reduce the P_f to less than 0.01 W per cell, the 80 mg finger wet weight requires at least 8 busbars, the 40 mg finger wet weight requires at least 11 busbars, and the 20 mg finger wet weight requires at least 15 busbars.

The half-cell or one-third-cell designs will lead to a sharp decrease in the production rate of the soldering process and increase the module costs. However, the conductive belt technology can remove the soldering process. Therefore, the costs for half-cell or one-third-cell modules with conductive belt are acceptable.

In order to achieve an acceptable cell breakage rate, the wires cannot be too thick. For those cells with a conventional thickness of about 180 μm, the present acceptable wire diameter is no more than 200 μm. The conductive belt technology will be developed continuously to apply thicker wires. On the other hand, cells will become thinner, and the wires had better be finer to maintain the cell breakage rate. For full, half, and one-third cell designs, and for the maximum diameters of 100 μm, 200 μm, and 300 μm, the P_c of a module with cell area equal to a full cell was calculated, and the results are shown in Figure 12. As the wires become finer, P_c increases sharply, and the wire number at the lowest P_c also increases. If the maximum diameter is 200 μm or 300 μm, the lowest P_c of half-cell design has a great advantage compared to full-cell design. One-third-cell design can decrease P_c by less than 0.043 W compared to the half-cell design. One-third-cell design needs one more cell separation per cell compared with half-cell design, and the power loss caused by a cell separation is more than 0.02 W. On the other hand, one-third-cell design also needs a more production process. Thus, one-third-cell design is not so economical. However, if the wire diameter decreases to less than 100 μm, P_c would increase sharply, and one-third-cell would be a better choice.

Define $P_t = P_f + P_c$. As calculated above, for the cell thickness and the conductive belts at current technologies, half cells combined with 200 μm-thick wire can achieve the lowest P_t. Moreover, for the finger wet weights of 80 mg, 40 mg, and 20 mg, the P_t for different numbers of wires was calculated. The results are shown in Figure 13. The shading rate of the interconnection ribbons with a width of 1.2 mm was tested by the same method shown in Section 2.2. P_t for a conventional four-busbar one-full-cell module with a finger wet weight of 80 mg was calculated, and the result is also shown in Figure 13.

For full-cell and multibusbar structures, the most relevant contribution to P_t is that of wires, while the finger resistance has a minor impact [3]. We can get the same

conclusion from Figure 13. However, as the cell cut to 1/2 or 1/3, P_c will drop sharply. For the finger wet weights of 80 mg, 40 mg, and 20 mg, the wire numbers for the lowest P_t are 13, 14, and 16, and the differences between these lowest P_t are less than 0.01 W. Therefore, if the busbar number increases to more than 13, the 20 mg wet weight will barely decrease the module power output. As shown in Figure 13, compared with a conventional four-busbar module with a full cell, the P_t of a 16-busbar module with two half-cells can be decreased by at least 0.19 W and can save 75% of the front finger silver paste. In other words, compared with the conventional four-busbar module with 72 full cells, the multibusbar and half-cell (MBBHC) module, which has 16 busbars and 144 half cells, can increase P_m by 13.68 W.

In addition, the MBBHC structure achieved with conductive belts can further increase P_m in the following ways: (1) The silver paste on the front and back busbar areas is removed, which will reduce the surface recombination and improve the V_{oc} of the cell [29]. (2) The backplane between the gaps of the half cells can reflect the light back to the cell, which can increase the P_m of a module with 144 half cells by 10 W [19]. (3) It is difficult for conventional screen printing to further decrease the finger width because of more broken fingers. Modules with 16 busbars can tolerate more broken fingers because P_f is reduced sharply. Therefore, the width of the fingers can be reduced to less than 40 μm by conventional screen printing, which will increase P_m by at least 0.05 W per cell.

5. Reliability Analysis of Multibusbar Modules Made with Conductive Belts

The materials applied in the modules except the cells and the conductive belts are the same as conventional modules. The cell metallization pattern will be optimized by applying conductive belt technology, but this may not reduce the cell reliability. Thus, the module reliability analysis should focus on the reliability of the conductive belt. As the conductive belts are encapsulated inside the module, the main relevant factors that may affect them are the module temperature and the incident ultraviolet, and the reliability tests of the conductive belts mainly include two aspects: (1) the wire contact resistance to fingers and Al-BSF and (2) the shading loss of the conductive belt.

Twenty conventional four-busbar monocrystalline solar cells were made into one-cell modules, respectively, by applying conductive belts, and the front and the back structure were the same as those in Figures 5(a) and 5(c). The wire contact resistance to fingers and Al-BSF were tested using the same method described in Section 2.3, and the results are shown in Figure 14. The following aging tests for the 20 modules were conducted: (1) ultraviolet aging test, which required 85°C and 200 W/m^2 ultraviolet power for 1000 hours, (2) thermal cycling test, which required temperature cycling between 85°C and −40°C for 200 cycles, and (3) damp heat test, which required 85°C and 85% relative humidity for 1000 hours. After aging tests, the wire contact resistance to fingers and to Al-BSF were tested again. As shown in Figure 14, after aging tests, the average wire contact resistance

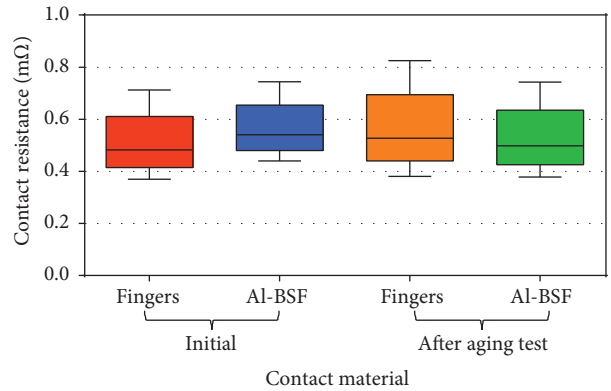

Figure 14: The wire contact resistances to fingers and Al-BSF, which were tested initially and after aging tests.

to fingers and Al-BSF were between 0.4 mΩ and 0.6 mΩ and were almost unchanged. The module series resistance included three parts: (1) the series resistance of the cell, (2) the wire contact resistance to fingers and Al-BSF, and (3) the series resistance of the wires. The wire resistance tested initially and after aging tests were also unchanged. Thus, the series resistance of the modules with conductive belts will not increase after aging tests.

Another two groups of modules were made to test the degradations of the electrical properties caused by the aging tests. Each group had four modules, which were composed of four conventional half cells, respectively. The half cells were chosen from the same batch and were not used before this experiment. I_m and P_m of the half cells were tested and were nearly equal. In group 1, the half cells were serially connected by interconnection ribbons, and in group 2, the half cells were serially connected by conductive belts. The conductive belts had 12 wires, respectively, and the diameter of the wires was 200 μm. The other materials applied in the two groups of modules were the same.

The aging tests shown above were made to these modules again, and after aging tests, there were almost no changes in the appearances of the modules. The appearance and electroluminescence (EL) images of a second group module after aging tests are shown in Figures 15(a) and 15(b). As shown in Figure 15(b), the wires and the fingers kept a uniform contact effect after aging tests. Thus, the wires could collect the cell current at each contact point.

Before and after aging tests, the I–V curves of the modules were tested. For the two groups, the average degradations of P_m, I_{sc}, V_{oc}, FF, R_s (ΔP_m, ΔI_{sc}, ΔV_{oc}, ΔFF, and ΔR_s were calculated, and the results are shown in Table 2. The degradations in the modules made with conductive belts were slightly less than in the conventional modules and were below the 5% maximum degradation prescribed by International Electrotechnical Commission (IEC) standards. The shading rate of the conductive belt may affect I_{sc}. The I_{sc} degradation of group 2 was less than that of group 1 and was less than 5%. Thus, the shading loss of the conductive belt did not increase after aging tests, or its incensement was acceptable.

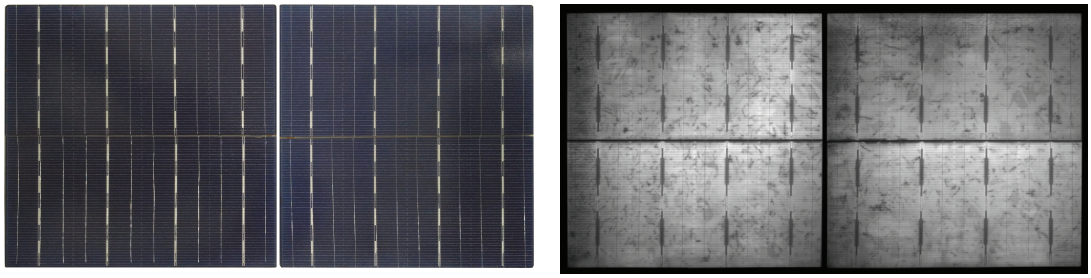

(a) (b)

Figure 15: The appearance (a) and EL image (b) of a module made with conductive belts and four half cells after aging tests.

Table 2: The average degradations of the module electric performance after aging tests: group 1, conventional four-busbar modules; group 2, modules made with conductive belts.

Group number	ΔP_m (%)	ΔI_{sc} (%)	ΔV_{oc} (%)	ΔFF (%)	ΔR_s (mΩ)
1	3.77%	3.13%	0.54%	0.12%	−0.5
2	3.16%	2.62%	0.46%	0.10%	−0.2

6. Conclusion and Outlook

In this paper, we prepared an interconnect electrode called conductive belt to achieve a multibusbar structure and the conductive belt can form ohmic contacts with its wires to the cell electrode. The practical shading area of the conductive belt tested was about 70% of the wire covering area. The wire contact resistance to fingers and Al-BSF was so small that it could be ignored. Thus, the conductive belts could contact with fingers and Al-BSF directly, and the front and back busbars could be removed. For fingers with different numbers of wires, we tested the finger series resistance and found the relationship between the series resistance variation and the maximum power output in two ways. For the full-cell, half-cell, and one-third-cell designs, and for the finger wet weights of 80 mg, 40 mg, and 20 mg per full cell, we optimized the diameter and the number of the wires and got the lowest power loss of the module electrode. Because the capacity reduction brought about by the half cell could be relieved by applying conductive belts, half cells combined with sixteen 200 μm thick wires could achieve the maximum profit and could save 75% of the finger wet weight. We made aging tests and found that the reliability of the MBBHC modules made with conductive belts could meet IEC standards.

We have carried out an outdoor test for MBBHC modules for three months and will continue the test for more than one year. MBBHC modules will be prepared with optimized cell electrode patterns, and their electrical parameters will be investigated in practice.

Data Availability

The data used to support the findings of this study are available from the corresponding author upon request.

Conflicts of Interest

The authors declare that they have no conflicts of interest.

Acknowledgments

The authors gratefully acknowledge the financial support of the National Nature Science Foundation of China (Grant nos. 11404253 and 11404260).

References

[1] N. Chen and A. Ebong, "Towards 20% efficient industrial Al-BSF silicon solar cell with multiple busbars and fine gridlines," *Solar Energy Materials and Solar Cells*, vol. 146, pp. 107–113, 2016.

[2] S. Braun, G. Hahn, R. Nissler, C. Pönisch, and D. Habermann, "Multi-busbar solar cells and modules: high efficiencies and low silver consumption," *Energy Procedia*, vol. 38, pp. 334–339, 2013.

[3] M. Nicolai, M. Zanuccoli, P. Magnone et al., "Simulation study of multi-wire front contact grids for silicon solar cells," *Energy Procedia*, vol. 77, pp. 129–138, 2015.

[4] N. Chen, A. Chowdury, E. Ahmad, V. Unsur, and A. Ebong, "Assessing the impact of multi-busbars on metallization cost and efficiency of solar cells with digital inkjet-printed gridlines," in *2013 High Capacity Optical Networks and Emerging/Enabling Technologies*, pp. 60–65, Magosa, Cyprus, December 2013.

[5] Y. Yang, P. P. Altermatt, W. Zhu, X. Liang, and H. Shen, "Analysis of industrial c-Si solar cell's front metallization by advanced numerical simulation," *Progress in Photovoltaics: Research and Applications*, vol. 20, no. 4, pp. 490–500, 2012.

[6] S. Thibert, J. Jourdan, B. Bechevet, D. Chaussy, N. Reverdy-Bruas, and D. Beneventi, "Emitter requirements for nickel contacts on silicon solar cells-a simulation study," *Energy Procedia*, vol. 38, pp. 321–328, 2013.

[7] S. Braun, G. Micard, and G. Hahn, "Solar cell improvement by using a multi busbar design as front electrode," *Energy Procedia*, vol. 27, pp. 227–233, 2012.

[8] J. Walter, M. Tranitz, M. Volk, C. Ebert, and U. Eitner, "Multi-wire interconnection of busbar-free solar cells," *Energy Procedia*, vol. 55, pp. 380–388, 2014.

[9] S. Schindler, J. Schneider, C. Pönisch, R. Nissler, and D. Habermann, "Soldering process and material characterization of miniaturized contact structures of a newly developed multi busbar cell metallization concept," in *28th European*

Photovoltaic Solar Energy Conference and Exhibition, pp. 480–483, Villepinte, 2013.

[10] A. F. Dethlefsen, M. Volk, K. Ramspeck, and C. Buchner, "Reliability testing of multi-busbar modules," in *29th European Photovoltaic Solar Energy Conference and Exhibition*, pp. 3323–3326, Amsterdam, The Netherlands, 2014.

[11] Z. Li, P.-C. Hsiao, W. Zhang et al., "Patterning for plated heterojunction cells," *Energy Procedia*, vol. 67, pp. 76–83, 2015.

[12] Y. Yao, P. Papet, J. Hermans et al., "Module integration of solar cells with diverse metallization schemes enabled by SmartWire Connection Technology," in *2015 IEEE 42nd Photovoltaic Specialist Conference (PVSC)*, pp. 1–5, New Orleans, LA, USA, June 2015.

[13] T. Söderström, Y. Yao, R. Grischke et al., "Low cost high energy yield solar module lines and Its applications," in *2015 IEEE 42nd Photovoltaic Specialist Conference (PVSC)*, pp. 1–6, New Orleans, LA, USA, June 2015.

[14] P. Papet, L. Andreetta, D. Lachenal et al., "New cell metallization patterns for heterojunction solar cells interconnected by the smart wire connection technology," *Energy Procedia*, vol. 67, pp. 203–209, 2015.

[15] J. Hermans, P. Papet, K. Pacheco et al., "Advanced metallization concepts by inkjet printing," in *29th European Photovoltaic Solar Energy Conference and Exhibition*, pp. 518–522, Amsterdam, 2014.

[16] S. Braun, R. Nissler, C. Ebert, D. Habermann, and G. Hahn, "High efficiency multi-busbar solar cells and modules," *IEEE Journal of Photovoltaics*, vol. 4, no. 1, pp. 148–153, 2014.

[17] A. B. Chebotareva, G. G. Untila, T. N. Kost, A. S. Stepanov, S. N. Salazkin, and V. V. Shaposhnikova, "Transparent conductive polymers for laminated multi-wire metallization of bifacial concentrator crystalline silicon solar cells with TCO layers," *Solar Energy Materials & Solar Cells*, vol. 165, pp. 1–8, 2017.

[18] G. G. Untila, T. N. Kost, A. B. Chebotareva et al., "Bifacial concentrator Ag-free crystalline n-type Si solar cell," *Progress in Photovoltaics: Research and Applications*, vol. 23, no. 5, pp. 600–610, 2015.

[19] S. Guo, J. Schneider, F. Lu et al., "Investigation of the short-circuit current increase for PV modules using halved silicon wafer solar cells," *Solar Energy Materials & Solar Cells*, vol. 133, pp. 240–247, 2015.

[20] J. Schneider, S. Schönfelder, S. Dietrich, and M. Turek, "Solar module with half size solar cells," in *29th European Photovoltaic Solar Energy Conference and Exhibition*, pp. 185–189, Amsterdam, The Netherlands, 2014.

[21] S. Eiternick, K. Kaufmann, J. Schneider, and M. Turek, "Loss analysis for laser separated solar cells," *Energy Procedia*, vol. 55, pp. 326–330, 2014.

[22] S. Eiternick, F. Kaule, H.-U. Zühlke et al., "High quality half-cell processing using thermal laser separation," *Energy Procedia*, vol. 77, pp. 340–345, 2015.

[23] S. Malik, D. Dassler, J. Fröbel, J. Schneider, and M. Ebert, "Outdoor data evaluation of half-/full-cell modules with regard to measurement uncertainties and the application of statistical methods," in *29th European Photovoltaic Solar Energy Conference and Exhibition*, pp. 3269–3273, Amsterdam, The Netherlands, 2014.

[24] S. Braun, G. Hahn, R. Nissler, C. Pönisch, and D. Habermann, "The multi-busbar design: an overview," *Energy Procedia*, vol. 43, pp. 86–92, 2013.

[25] D. Pysch, A. Mette, and S. W. Glunz, "A review and comparison of different methods to determine the series resistance of solar cells," *Solar Energy Materials & Solar Cells*, vol. 91, no. 18, pp. 1698–1706, 2007.

[26] A. Herguth, S. Braun, G. Hahn, C. Pönisch, and R. Nissler, "Towards non-permanent contacting schemes for busbar-free solar cells," in *28th European Photovoltaic Solar Energy Conference and Exhibition*, pp. 846–850, Paris, September-October 2013.

[27] J. Müller, D. Hinken, S. Blankemeyer et al., "Resistive power loss analysis of PV modules made from halved 15.6 × 15.6 cm^2 silicon PERC solar cells with efficiencies up to 20.0%," *IEEE Journal of Photovoltaics*, vol. 5, no. 1, pp. 189–194, 2015.

[28] Y. K. Fang, S. M. Sze, S. Cohen et al., "Contact resistance: its measurement and relative importance to power loss in a solar cell," *IEEE Transactions on Electron Devices*, vol. 31, no. 5, pp. 647–653, 1984.

[29] M. T. Zarmai, N. N. Ekere, C. F. Oduoza, and E. H. Amalu, "A review of interconnection technologies for improved crystalline silicon solar cell photovoltaic module assembly," *Applied Energy*, vol. 154, pp. 173–182, 2015.